

Dual frequency VSOP imaging of the jet in S5 0836+710

Andrei LOBANOV, Thomas KRICHBAUM, Arno WITZEL and J. Anton ZENSUS
Max-Planck-Institut für Radioastronomie, Auf dem Hügel 69, 53121
alobanov@mpifr-bonn.mpg.de

(Received 2000 December 31; accepted 2001 January 1)

Abstract

The luminous high-redshift ($z = 2.17$) quasar S5 0836+710 has been observed in October 1997 with the VSOP at 1.6 GHz and 5 GHz. We report here a previously unpublished image made from the data at 1.6 GHz and compare the structure of a relativistic jet in this quasar at the two frequencies. We present a spectral index image tracing spectral properties of the jet up to ~ 40 milliarcsecond distance from the nucleus. The curved jet ridge line observed in the images and the spectral index distribution can be described by Kelvin-Helmholtz instability developing in a relativistic outflow with a Mach number of ~ 6 . In this description, the overall ridge line of the jet is formed by the helical surface mode of Kelvin-Helmholtz instability, while areas of flatter spectral index embedded into the flow correspond to pressure enhancements produced by the elliptical surface mode of the instability. An alternative explanation involving a sequence of slowly dissipating shocks cannot be ruled out at this point.

Key words: galaxies: quasars: individual: 0836+710, galaxies: jets, galaxies: nuclei

1. Introduction

The VSOP (VLBI¹ Space Observatory Program) is the first Space VLBI (SVLBI) mission that has been running in a facility mode. VSOP observations have utilized a worldwide array of radio telescopes and an orbiting 8-meter antenna deployed on the Japanese satellite HALCA² (Hirabayashi 1996). It has been demonstrated that the ground-space baselines provided by HALCA contain a unique information about source structure, and that this information cannot be obtained by super-resolution applied to ground VLBI images (Lobanov et al. 1999; Murphy 1999). Regular VSOP observations started in September 1997 at 1.6 and 5 GHz, quickly turning it to an excellent tool to study the morphology extragalactic flows *en mass* (Scott et al. 2004, and references therein) and on a case by case basis (e.g., Hirabayashi, Edwards & Murphy 2000; Piner et al. 1999; Bower & Baker 2000; Jin et al. 2001; Lobanov et al. 2001; Lobanov & Zensus 2001). VSOP observations at 1.6 GHz match closely the resolution of the VLBA³ array at 5 GHz (Zensus, Diamond, & Napier 1995, and references therein). This can be used effectively for studying the distribution of spectral index in extragalactic jets (Edwards et al. 2001). The quasar 0836+710 (4C71.07, $z=2.17$) was observed with the VSOP in 1997, on October 3 (at 1.6 GHz) and October 7 (at 5 GHz). The observation at 5 GHz was presented in Lobanov et al. (1998).

0836+710 is an ultra-luminous quasar showing correlated (Otterbein et al. 1998) broad-band variability

in gamma-ray (Fichtel et al. 1994), X-ray (Brunner et al. 1994), optical (von Linde et al. 1993; Villata et al. 1997), mm- and cm- radio regimes (Marscher & Bloom 1994). The source has a well collimated VLBI-scale jet (Hutchison, Cawthorne & Gabuzda 2001; Zensus et al. 2002) extending out to ~ 240 milliarcseconds (Hummel et al. 1992). The jet shows typical proper motions of 0.2–0.3 mas/yr (Otterbein et al. 1998; Jorstad et al. 2001) and it is substantially curved, with lateral displacements of its ridge line and oscillations of its transverse width (possibly correlated with the observed jet speeds; Krichbaum et al. 1990).

We present here a 1.1-mas resolution VSOP image of 0836+710 made at 1.6 GHz, and discuss the morphological and spectral properties of the compact jet in this quasar. For the purpose of facilitating comparisons with previous measurements, the big bang cosmology with the Hubble constant $H_0 = 100 h \text{ km s}^{-1} \text{ Mpc}^{-1}$ and deceleration parameter $q_0 = 0.5$ is adopted throughout the paper. For 0836+710, this translates into a linear scale of 4.0 pc/mas and corresponds to apparent speed of $41.6c$ for an observed proper motion of 1 mas/yr.

2. VSOP observations and data reduction

0836+710 was observed with the VSOP at 1.6 GHz for 11.5 hours with the VLBA providing ground support for the observation. The data were recorded in the VLBA format, using total observing bandwidth of 32 MHz divided in two intermediate frequency (IF) bands, each having 256 spectral channels. The data were correlated at the VLBA correlator in Socorro, with output pre-averaging time of 1.966 and 0.524 seconds for the ground and space baselines respectively. Data from HALCA were received for the total of 5 hours at the satellite data acquisition

¹ Very Long Baseline Interferometry

² Highly Advanced Laboratory for Communication and Astronomy

³ Very Long Baseline Array of the National Radio Astronomy Observatory, USA

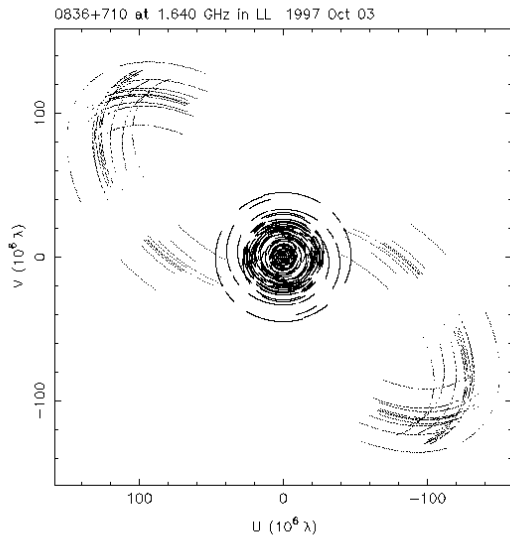


Fig. 1. The uv -coverage the VSOP observation of 0836+710. The inner circles correspond to the baselines between ground radio telescopes; the space baselines are grouped into larger ellipses extending at a P.A. $\approx 45^\circ$.

stations in Tidbinbilla (Australia), Robledo (Spain), and Green Bank (USA). Fringe visibilities were detected in the HALCA data recorded at all three STS. The RMS noise on the HALCA baselines is about 4.5 times higher than on the ground baselines. The uv -coverage of the final correlated dataset is shown in Fig. 1. The minimum uv -spacing of the data is $0.77 M\lambda$, corresponding to an angular scale of 260 mas. The maximum uv -spacings of the ground and space baselines are $47 M\lambda$ and $180 M\lambda$, respectively. These values indicate that the VSOP data provide an improvement of resolution by a factor of ~ 3.5 compared to ground VLBI observations at the same frequency. The estimated thermal RMS noise of the VSOP data is 0.75 mJy/beam , corresponding to a brightness temperature of $1.1 \times 10^6 \text{ K}$.

2.1. Fringe fitting

The correlated data were fringe-fit and imaged using AIPS⁴ and DIFMAP (Shepherd et al. 1994). Antenna gain and system temperature measurements were applied to calibrate the visibility amplitudes. After inspecting the IF bandpasses, the last 46 channels were flagged in each IF, owing to significant (50-80%) amplitude reduction. This has reduced the total observing bandwidth to 26.2 MHz. The recorded phase-calibration signals from the observing log were applied to the VLBA antennas. The residual delays and rates were corrected using the single-band (SB) and multi-band (MB) delay fringe fitting. We used solution intervals of 3 minutes (SB) and 5 (MB) minutes, and accepted all solutions with $\text{SNR} > 7$. After the fringe fitting, the residual phase variations were

Table 1. Parameters of the images in Fig. 1

Image	S_t	S_p	S_l	S_n	σ_r	D_r
VLBA	3950	1580	2.0	3.2	0.6	6500:1
VSOP	3780	600	6.0	7.0	1.5	2500:1

Notes: S_t [mJy] – total CLEAN flux density; S_p [mJy/beam] – peak flux density; S_l [mJy/beam] – lowest positive contour level in the image; S_n [mJy/beam] – largest absolute residual flux density; σ_r [mJy/beam] – residual rms noise; D_r – peak-to-rms dynamic range.

found to be within 2° on the ground baselines, and $< 10^\circ$ on the space baselines. We then averaged over all frequency channels, and calibrated the phases with a point source model (to enable time averaging).

2.2. Self-calibration and imaging

After fringe fitting, the data were exported into DIFMAP and further time-averaged into 60-second bins (with the resulting spatial dynamic range of ≈ 190 and the largest detectable scale of $\approx 270 \text{ mas}$). The amplitude and phase errors were calculated from the scatter in the un-averaged data. The hybrid imaging using the CLEAN algorithm was applied to produce final, self-calibrated images. Both phase and amplitude self-calibration have been applied, with amplitudes being allowed to vary only after the total model flux has approached the zero spacing flux to within 3%.

To evaluate and compare the quality of the VSOP data to that of the ground VLBI observations, we produce two different images: a “VSOP image” made from the entire dataset and a “VLBA image” obtained from the visibility data measured between the ground telescopes. Natural weighting is applied for gridding the ground array data, enhancing the sensitivity to extended emission at the price of slightly decreased image resolution. The gridding weights are also scaled by amplitude errors raised to the power of -1 . Uniform weighting is applied for gridding the full-resolution VSOP data, which provides a better angular resolution at the expense of lowering slightly the sensitivity to extended structures. In the VSOP data, scaling the gridding weights by the amplitude errors weights down significantly all of the long uv -spacings, since the noise on HALCA baselines is much higher than on the ground baselines. To avoid the down-weighting of the HALCA baselines, the amplitude scaling of gridding weights is switched off. As a safeguard measure, only phase self-calibration is applied to the VSOP dataset. After a good fit to the data is achieved, the antenna gains are adjusted, correcting for small constant offsets between the model and the visibility amplitudes. Fig. 2 presents the VLBA image and a the VSOP image of 0836+710 obtained using this procedure. Table 1 lists basic parameters of the two images.

The quality of the images can be assessed from the residual rms, σ_r , and the maximum amplitude, S_r , in the residual image. Assuming that the ideal, theoretical noise is Gaussian, with a zero mean, the measured σ_r can be used to estimate the expected value of S_r in a residual image

⁴ The NRAO Astronomical Image Processing System

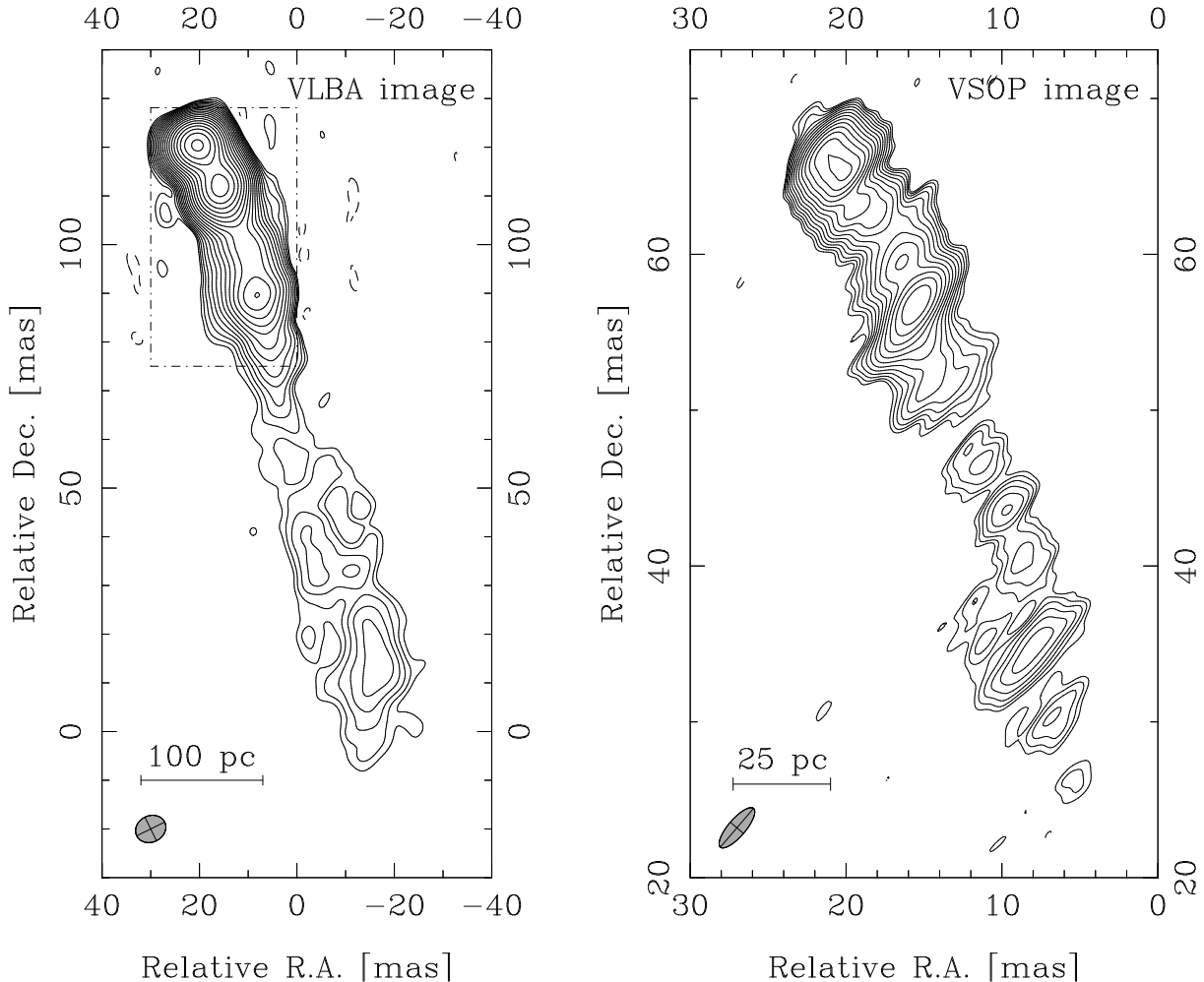


Fig. 2. Ground array VLBA image (left) and VSOP image (right) of 0836+710 at 1.6 GHz. In the VLBA image, the dotted-line rectangle shows the area covered by the VSOP image. The image parameters are summarized in Table 1. Contours are drawn at $-1, 1, \sqrt{2}, 2, \dots$ of the respective lowest contour levels, S_1 listed in Table 1. The respective synthesised beams and linear scales are drawn in the bottom-left corner of each image. The synthesised beam in the VLBA image is 6.4×5.4 mas at a P.A. of $-63^\circ 9$. The synthesised beam in the VSOP image is 3.3×1.1 mas at a P.A. of $-40^\circ 6$.

$$|S_{r,\text{exp}}| = \sigma_r \left[\sqrt{2} \ln \left(\frac{N_{\text{pix}}}{\sqrt{2\pi}\sigma_r} \right) \right]^{1/2},$$

where N_{pix} is the total number of pixels in the image. For the images of 0836+710, $N_{\text{pix}} = 1024^2$, and the expected values of S_r are 2.6 mJy/beam and 6.3 mJy/beam for the VLBA and the VSOP image, respectively. The ratio $\epsilon_r = S_r/S_{r,\text{exp}}$ expresses the quality of the residual noise distribution. Ideally ϵ_r should be close to unity. Large values of ϵ_r indicate that not all the structure has been adequately recovered, while small values of ϵ_r imply that the number of degrees of freedom in the model representation of the emission is too large. A relative deviation of the measured noise distribution from the ideal, Gaussian noise is then given by $\kappa_\sigma = \exp(|\ln \epsilon_r|) - 1$, in units of the Gaussian standard deviation, σ . This yields $\kappa_\sigma(\text{VLBA}) = 0.23\sigma$ and $\kappa_\sigma(\text{VSOP}) = 0.11\sigma$, indicating that the distributions of residual noise are sufficiently close to the Gaussian distribution. This implies that both images adequately represent the structure detected in the

visibility data.

3. Morphology and spectrum of the jet

In both images in Fig. 2, the jet is continuous and curved, with several enhanced emission regions embedded in it. The apparent curvature of the jet may reflect the presence of plasma instabilities in the jet (e.g. MHD or Kelvin-Helmholtz instabilities). Note the roughly two times smaller dynamic range of the VSOP image (2500:1, compared to 6500:1 obtained in the VLBA image) caused by the poorer sampling and increased noise of the data on the space baselines. Such a reduction of the dynamic range is typical for all VSOP observations. One can compare the result above with the VSOP observation of 0836+710 at 5 GHz (Lobanov et al. 1998) which yielded the dynamic ranges of the ground and space images at 5 GHz are 4600:1 and 900:1, respectively.

In Fig. 3, the images at 1.6 GHz and 5 GHz are com-

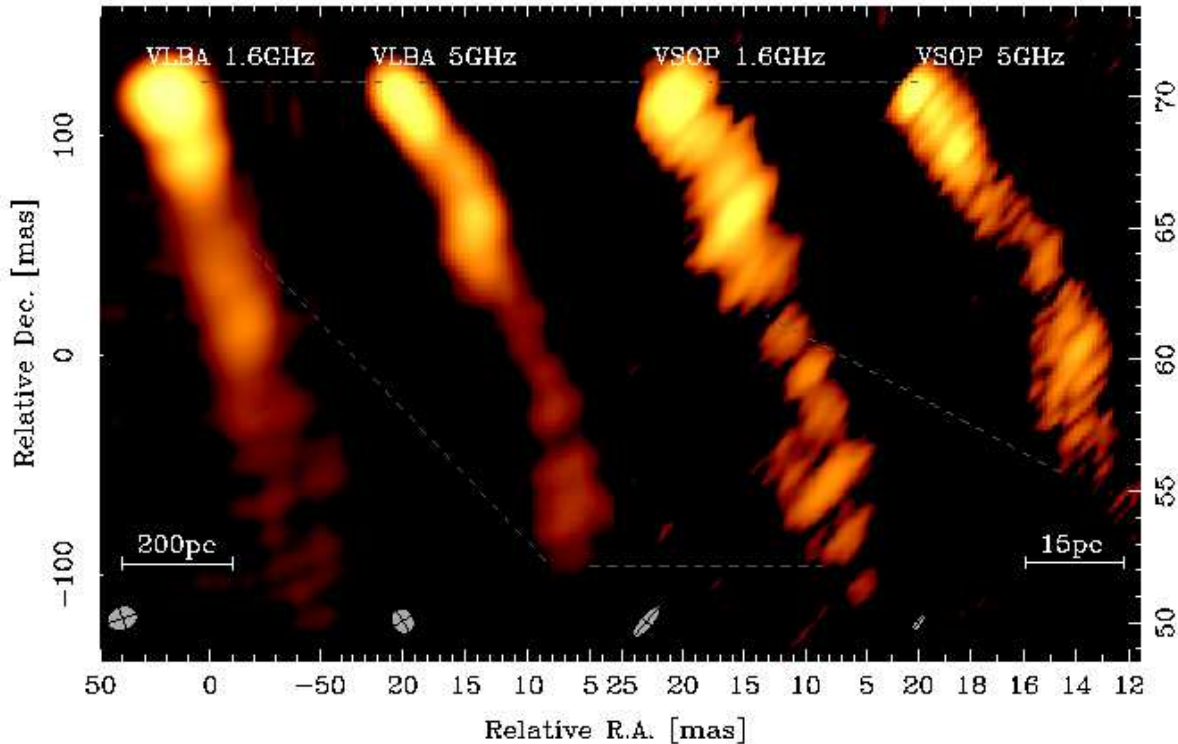


Fig. 3. Collage of the VLBA and VSOP images at 1.6GHz and 5GHz. Tick marks along the R.A. axis give relative scale and position of the emission in the individual images. In each individual image, the scales of the respective R.A. and Dec. axis are equal. The Declination axes are marked explicitly for the 1.6 GHz VLBA image (left side) and 5GHz VSOP image (right side). Dashed lines indicate similar scales in different images. Ellipses mark the synthesised beams of each individual image, plotted to the respective scales. The 1.6 GHz VLBA image is made with a Gaussian taper of 0.5 at $u \geq 10 M\lambda$ to emphasize structures on scales ≥ 100 mas (the un-tapered image is shown in the left panel of Fig. 1). The synthesised beam of the tapered image is 14.5×11.2 mas at a P.A. of -71° . Formal parameters and a detailed discussion of the images at 5 GHz are given in Lobanov et al. (1998). The VLBA image at 5 GHz and the VSOP image at 1.6 GHz have comparable synthesised beams due to roughly matching uv -coverages. These images can be used for mapping the spectral index distribution in the jet.

pared, illustrating the large magnitude of angular scales probed by ground and space VLBI data. The jet oscillates with respect to the general direction of the jet axis at a P.A. $\approx 162^\circ$. In the heavily tapered VLBA image at 1.6 GHz, the jet is traced up to ~ 240 mas ($960 h^{-1}$ pc), similar to the extent of the emission recovered in the previous VLBI+MERLIN observations of 0836+710 (Hummel et al. 1992). The VSOP image at 5 GHz (Lobanov et al. 1998) shows the fine structure on scales down to $\approx 0.8 h^{-1}$ pc. The VLBA image at 5 GHz has a resolving beam of 2.15×1.75 mas that is similar to the synthesised beam of the VSOP image at 1.6 GHz. The VSOP beam is more elongated, but the two beams have almost identical area (2.96 mas^2 and 2.85 mas^2 , respectively). This facilitates making a spectral index map from these images.

3.1. Spectral index distribution

To derive the distribution of spectral index between 1.6 GHz and 5 GHz we restore both individual images with a circular beam of 2.5 mas in diameter (actually increasing the beam area by a factor of ≈ 1.7 compared to the original synthesised beams). Natural weighting was used for producing the image at 5 GHz and the gridding weights

were scaled by the amplitude errors raised to the power of -2 . The image at 1.6 GHz was produced with the uniform weighting and without scaling the gridding weights by the amplitude errors. The resulting images are shown in the upper left panels of Fig. 4 and their properties are summarized in Table 2.

The images were aligned at the position of the peak of the brightest secondary feature (near the outer edge of the region J2 marked in images in Fig. 4). This measure is intended to reduce the effect of the variable optical depth across the nuclear region. To produce the alignment, the 5.0 GHz image was shifted by 1.2 mas and 1.6 mas in right ascension and declination, respectively. It should be noted that this shift does not correspond directly to the core shift due to self-absorption of synchrotron emission (Lobanov 1998a), since a fraction of it comes from the shift of the phase-center of the 1.6 GHz VSOP image in which the peak brightness is observed downstream from the jet base. Accurate model-fitting analysis is required to assess the amount of core shift due to opacity in the nuclear region. A preliminary estimate indicates a likely shift of 0.8–1.2 mas.

After the alignment, the spectral index was calculated

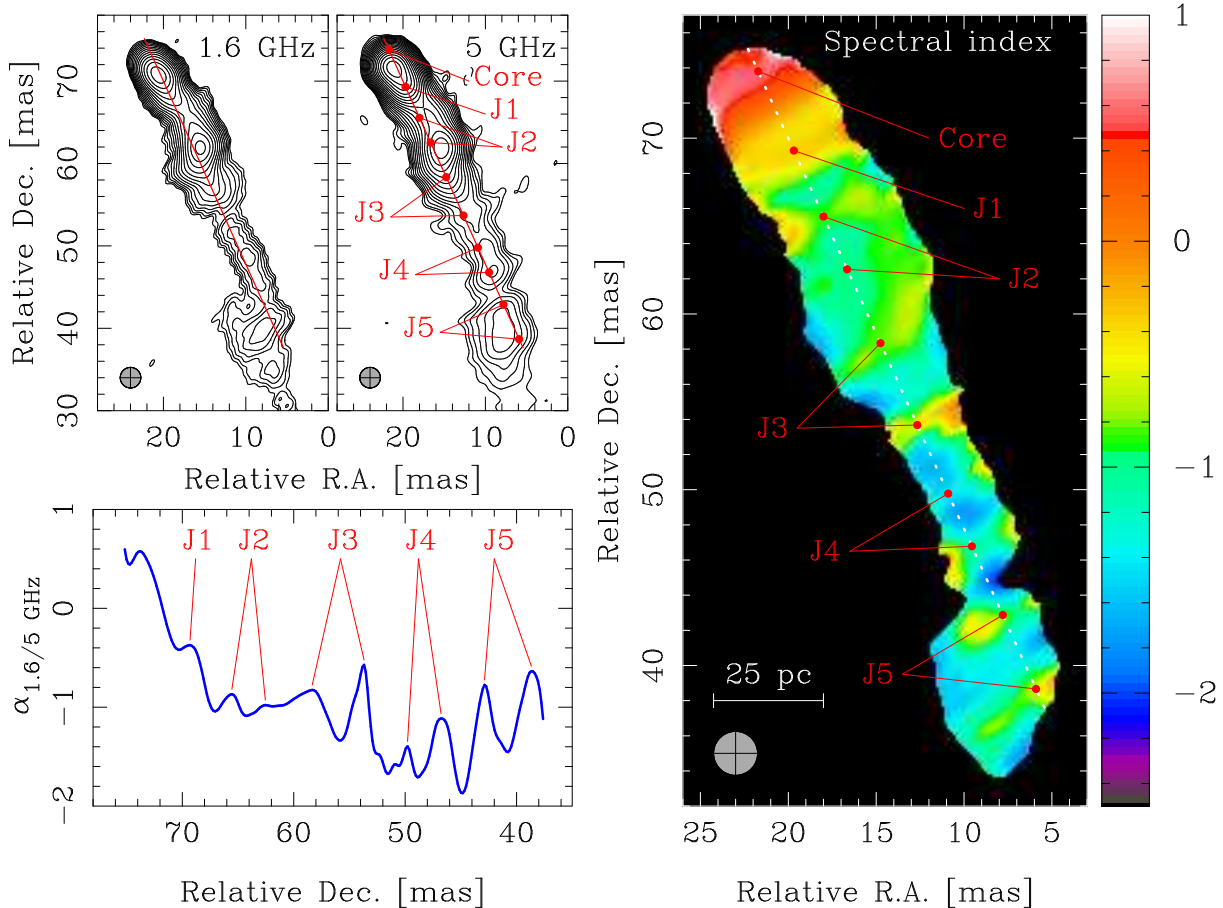


Fig. 4. Spectral index distribution in the jet of 0836+710. The distribution is derived from the images shown in the top left. The ground array image at 5 GHz and VSOP image at 1.6 GHz have comparable synthesised beams that facilitate spectral index mapping. The restoring beam is a circular Gaussian with a diameter of 2.5 mas. The two images are aligned at the position of the peak in the region J2 (to avoid the frequency dependence of the apparent location of the nucleus of the jet; Lobanov 1998a). The resulting spectral index distribution is shown in the right panel. The spectral index varies smoothly along the jet and shows largely transverse structure indicative of shocks. The spectrum remains optically thick within ≈ 7 mas from the nucleus. Dotted line marks the run of a slice presented in the bottom left panel. Dots indicate the locations of individual peaks identified in the slice. In the optically thin part of the jet, edges of all distinct regions of enhanced emission (marked with a letter “J” and successive numbers) are emphasized by peaks of the spectral index. The peaks are spaced at quasi-regular intervals, with an average separation of 4.8 ± 0.2 mas. This regularity is indicative of shocks or instabilities developing in the jet plasma.

in all pixels with flux densities larger than 5 mJy/beam and 3 mJy/beam in the 1.6 GHz and 5 GHz images, respectively. The resulting spectral index image is shown in the right panel of Fig. 4. The image shows a smooth distribution of spectral index on angular scales of up to 40 mas ($160h^{-1}$ pc). The spectral index varies from +0.6 in the optically thick nuclear region to -1.8 in the rarefied, optically thin regions of the extended jet. Most of the distinct features visible in the spectral index map are oriented roughly transversely to the jet, outlining a smooth and regular evolution of the spectral index along the flow. The optically thick emission extending up to ≈ 7 mas ($\approx 30h^{-1}$ pc distance from the base of the jet is likely to mark the region where radiation from strong shocks dominates. This scale is similar to the one found in 3C 345 (Lobanov & Zensus 1999), from spectral evolution in the regions of enhanced emission (jet components).

To illustrate the connection between the spectral index

Table 2. Parameters of the single frequency images in Fig. 4

Image	S_t	S_p	S_l	S_n	σ_r	D_r	S_{cl}
1.6GHz	3780	1140	7.0	7.0	1.4	2700:1	5.0
5GHz	2160	1000	1.5	6.2	0.4	5400:1	3.0

Notes: S_t [mJy] – total CLEAN flux density; S_p [mJy/beam] – peak flux density; S_l [mJy/beam] – lowest positive contour level in the image; S_n [mJy/beam] – largest absolute residual flux density; σ_r [mJy/beam] – residual rms noise; D_r – peak-to-rms dynamic range; S_{cl} [mJy/beam] – flux density clipping level for the spectral index map.

distribution and the regions of enhanced brightness embedded in the jet, a run of the spectral index along a slice in the jet is plotted in the lower left panel of Fig. 4. The location of the slice is indicated in the spectral index map and in the 5 GHz image. The dots mark the positions of the local peaks in the run of the spectral index. The peaks seemingly underline the edges of the enhanced emission regions. This can be viewed as evidence for forward and reverse shocks dissipating in the jet after injection of dense plasma condensations at the nucleus (cf., Marscher & Bloom 1994; Aloy et al. 2003). The likely associations with the enhanced brightness regions are marked with J1–J5 in Fig. 4. Another possible explanation involves elliptical modes of Kelvin-Helmholtz (K-H) instability developing in the flow (Hardee 2000; Lobanov & Zensus 2001). It is remarkable that the peaks in the spectral index run are separated by similar intervals, with an average separation of 4.8 ± 0.2 mas. This regularity suggests that K-H instability can also play a role in forming the observed structure. It is also possible that the observed morphology and spectral properties result from an interplay between relativistic shocks and instabilities (Lobanov & Zensus 1999). Better indications about the nature of the extended emission should come from imaging the turnover frequency distribution (Lobanov 1998b), which is sensitive to velocity and pressure gradients in the plasma.

4. Discussion

The reported observation of 0836+710 shows that the VSOP mission provides an excellent opportunity for high-resolution and high dynamic range imaging of VLBI-scale jets in extragalactic objects. The VSOP image of 0836+710 allows to investigate the jet morphology and physical conditions on projected linear scales up to 1 kpc. The jet is substantially curved on scales from ~ 2 mas to ~ 100 mas, underlining the likely complexity and possible stratification of the flow. This is also reflected in remarkable changes of the apparent speeds measured at different locations along the jet. Near the core, apparent speeds $\beta_{\text{app}} \approx 10 h^{-1} c$ are measured. At a 3 mas core separation, the speed decreases down to $\beta_{\text{app}} \sim 2\text{--}3 h^{-1} c$, and then becomes larger once again, further out (Krichbaum et al. 1990; Otterbein 1996).

This kinematic behavior and the pronounced curvature of the jet are indicative of Kelvin-Helmholtz (K-H) instability developing in the flow (Hummel et al. 1992). Previous analysis of the jet ridge line measured in the VSOP image at 5 GHz (rightmost image in Fig. 3) has indicated that, on scales of ≤ 20 mas the jet is dominated by a helical surface (H_s) mode of K-H instability (Hardee 2000) in a relativistic flow with a Lorentz factor $\Gamma_j \approx 11$, Mach number $M_j \approx 6$, and a jet/ambient medium density ratio of ≈ 0.04 (Lobanov et al. 1998). With the parameters derived in Lobanov et al. (1998), the H_s mode has a wavelength of ≈ 7.7 mas, similar to the oscillations observed in the ridge line at 5 GHz. The corresponding wavelength of the elliptical surface mode (E_s) is ≈ 4.6 mas, which is close to the observed aver-

age separation of 4.8 ± 0.2 mas between the peaks in the spectral index run (bottom left panel of Fig. 4). The instability should have a relatively fast propagation speed $\beta_w \approx 0.7 c$. To maintain the remarkable stability of the flow, the opening angle, ϕ_j , of the jet should not exceed the limit of $1/(\Gamma_j M_j)$, which translates into $\phi_j \lesssim 1^\circ$.

The VLBA image at 1.6 GHz (left panel of Fig. 2) gives an hint of a structural changes at a much longer wavelength, possibly as large as ~ 100 mas. It is impossible to reproduce this wavelength in a flow discussed above, as it would require the jet to have an opening angle far in excess of the 1° limit derived above. This implies that either this wavelength is either produced in a flow with substantially different properties (for instance, it could be generated in outer layers of a stratified flow) or it is not related to K-H instability at all (it could be due to precession or other purely kinematic factors). This is subject to a more detailed analysis of the morphology and kinematics of the jet. At this point, it could only be noted that such a wavelength could correspond to a helical surface mode of K-H instability developing in outer layers of the jet, with a transverse width about 10 times larger than the width of the flow giving rise to the shorter wavelengths detected in the VSOP image at 5 GHz.

Finally, the preliminary measurement of the core shift between 1.6 GHz and 5 GHz allow us to place limits on the parameters of the inner jet, following the method described in Lobanov (1998a). The magnetic field strength in the self-absorbed core should be 2 mG and 18 mG at 1.6 GHz and 5 GHz, respectively (assuming the spectral index of -0.7 for synchrotron emission). The 1.6 GHz core should be located at about 85 pc (≈ 1 mas, assuming a viewing angle of 3°) from the central engine of the AGN. The total luminosity of the jet reaches up to 10^{48} erg/s, with about 10% of that coming from the synchrotron emission. This makes 0836+710 one of the most powerful extragalactic jets certainly worth of more detailed studies.

Acknowledgments

We gratefully acknowledge the VSOP Project, which is led by the Japanese Institute of Space and Astronautical Science in cooperation with many organizations and radio telescopes around the world. The National Radio Astronomy Observatory is a facility of the National Science Foundation operated under cooperative agreement by Associated Universities, Inc.

References

- Aloy, M.-A., Martí, J.-M., Gómez, J.L., et al. 2003, ApJ, 585, 109.
- Bower, G.C. & Baker, D.C. 2000, Advances in Space Research, 26, 731.
- Brunner H., Lamer G., Staubert R., Worall D. M., 1994, A&A 287, 436.
- Edwards, P.G., Giovannini, G., Cotton, W.D., et al. 2001, PASJ, 52, 1015.
- Fichtel C.E. Bertsch D.L., Chiang J. et al., 1994, ApJS, 94, 551.

- Hardee, P.E. 2000, ApJ, 533, 176.
- Hirabayashi, H. 1996, Springer Science (Quarterly) 2, 11, 6.
- Hirabayashi, H., Edwards, P.G. & Murphy, D.W. (eds.),
Astrophysical Phenomena Revealed by Space VLBI,
Proceedings of the VSOP Symposium (ISAS: Sagamihara),
2000
- Hummel C.A., Muxlow T.W.B., Krichbaum T. P. et al., 1992,
A&A, 266, 93.
- , Hutchison, J.M., Cawthorne, T.V. & Gabuzda, D.C. 2001,
MNRAS, 321, 525.
- Jin, C., Krichbaum, T.P., Witzel, A., et al. 2001, Ap&SS, 278,
97.
- Jorstad, S.G., Marscher, A.P., Mattox, J.R., et al. 2001, ApJS,
134, 181.
- Krichbaum T.P., Hummel C.A., Quirrenbach A. et al., 1990,
A&A, 230, 271.
- von Linde J., Borgeest U., Schramm K.-J. et al., 1993, A&A
267, L23.
- Lobanov, A.P. 1998a, A&A, 330, 79.
- Lobanov, A.P. 1998b, A&AS 132, 261.
- Lobanov, A.P., Krichbaum, T.P., Witzel, A., et al. 1998, A&A
340, 60.
- Lobanov, A.P. & Zensus, J.A. 1999, ApJ, 521, 509
- Lobanov, A.P., Krichbaum, T.P., Witzel, A. & Zensus, J.A.
1999, New Astronomy Reviews, 43, 741.
- Lobanov, A.P. & Zensus, J.A. 2001, Science, 294, 128.
- Lobanov, A.P., Gurvits, L.I., Frey, S., et al. 2001, ApJ, 547,
714.
- Marscher A.P. & Bloom S.D. 1994, in Compact Extragalactic
Radio Sources.
- Murphy, D.W. 1999, Advances in Space Research, 26, 609.
- Murphy, D.W., Tingay, S.J., Preston, R. A., et al. 1999,
Advances in Space Research, 26, 665
- Otterbein K., 1996, PhD thesis, University Göttingen.
- Otterbein K., Krichbaum, T. P., Kraus, A., et al. 1998, 334,
489.
- Piner, B.G., Unwin, S.C., Wehrle, A.E., et al. 199, ApJ, 525,
176.
- Scott, W.K., Fomalont, E.B., Horiuchi, S., et al. 2004, ApJS,
155, 33.
- Shepherd M. C., Pearson, T. J., & Taylor, G. B. 1994, BAAS
26, 987.
- Villata M., Raiteri C.M., Ghisellini G., et al. 1997, A&AS, 121,
119.
- Zensus, J. A., Diamond, P. J., & Napier, P. J. (eds.) 1995,
“Very Long Baseline Interferometry and the VLBA”, ASP
Conference Series, Vol. 82.
- Zensus, J.A., Ros, E., Kellermann, K.I., et al. 2002, AJ, 124,
662.